Reduced Rank Interference Suppression for Multichannel SAR

Luke Rosenberg, Doug Gray
University of Adelaide, Australia

Luke Rosenberg
Defence Science and Technology Organisation, Australia

Abstract

Large regions of a Synthetic Aperture Radar (SAR) image can potentially be destroyed by an airborne broadband jammer. Jammer components include both the direct-path and multipath reflections from the ground, known as hot-clutter (HC) or terrain scattered interference. Using multiple antennas on a SAR provides spatial degrees of freedom and allows for beamforming to reject the direct-path signal. Previous studies have shown that derivative constraints when combined with fast-time taps can suppress HC while maintaining a reasonable SAR image. This approach however requires an expensive matrix inverse and may not be implementable in real time. This paper therefore presents a fast-time Space Time Adaptive Processing (STAP) algorithm with a reduced rank constrained Generalised Sidelobe Canceller (GSC).

1 Introduction

The goal of interference suppression for SAR is to successfully suppress the unwanted signals while not significantly effecting the image quality by blurring, reducing the resolution or raising the sidelobe level. This can be hard to achieve in practice, especially if the interference is non-stationary and the training statistics change from pulse to pulse, causing traditional slow-time STAP techniques be ineffective, [1]. Therefore adapting within each pulse is required by exploiting spatial/fast-time STAP. This offers the advantage of exploiting the coherency between the direct-path jammer and other HC signals to provide improved interference rejection. It will however cause secondary modulations during image formation, similar to that shown by [2]. In previous work, the use of derivative constraints to reduce potential signal suppression has shown to be an effective compromise to reduce the interference without compromising the targets range profile, [3].

Fully adaptive processing can be very computationally intensive and not suitable for real time operation. Moreover, if the interference is non-stationary, the eigenvalues of the covariance matrix will spread, increasing the interference rank and therefore the degrees of freedom required to effectively cancel it. This problem is also analogous to the Moving Target Indication application where the ground clutter returns may not be stationary due to real world effects, such as aircraft crabbing, non-linear array geometry, intrinsic clutter motion, and scattering from near-field obstacles, [4].

Reduced rank techniques work to reduce the rank associated with the interference plus noise covariance matrix. Many of the methods in the literature promise performance near or better then their full rank counterparts but with reduced sample support and computation. This paper looks at applying space/fast-time adaptive algorithms to the problem of interference suppression in the presence of non-stationary HC. A constrained fast-time GSC is modified to use a lower rank covariance matrix similar to [5], with diagonal loading to achieve performance similar to the full rank derivative constraint implementation.

2 System Models and Geometry

2.1 SAR Signal Model

Consider a SAR platform travelling along the y-axis at v_p m/s, imaging a point in the slant-plane $x \in [X_c - X_0, X_c + X_0]$, $y \in [-Y_0, Y_0]$. The radar transmits a broadband chirp and the received signal $x_n(t,u)$, is base-banded and sampled for each of the N channels of a linear antenna array with equi-spaced receivers along the azimuth direction. The variables (t,u) represent (fast-time) samples within a pulse and the SAR platform position (slow-time) respectively. As the SAR bandwidth, B (Hz) is much smaller than the carrier frequency, ω_c (rad/s), the SAR signal model can be split into temporal and spatial components.

The spatial reference signal is given by the time difference between the phase centre of the antenna array and the n^{th} channel and can be approximated as a function of the SAR position u or equivalently, an angular offset $\theta(u)$, i.e.,

$$s_n(u) = \exp\left[j\frac{\omega_c}{c} d_n \sin\left[\theta(u)\right]\right] \tag{1}$$

where c is the speed of light, $\theta(u) = \arctan(u/X_c)$ is the steering angle and $d_n = n\delta$ is the antenna offset from the array phase centre with antenna spacing δ and $n \in [-(N-1)/2, (N-1)/2]$ for N (odd) antenna elements.

The received SAR signal comprises the total ground return, $\gamma_n(\cdot)$, interference from the direct-path and ground reflected path (HC), $z_n(\cdot)$ and receiver noise $\nu_n(\cdot)$.

$$x_n(t,u) = \gamma_n(t,u) + z_n(t,u) + \nu_n(t,u) \tag{2}$$

The noise signal $\nu_n(\cdot)$ represents the receiver noise for each channel. It is modelled as white Gaussian noise with zero mean and unity variance. Figure 1 shows the processing chain from transmission of the chirp signal, formation of the received SAR signal, range processing, adaption and image formation.

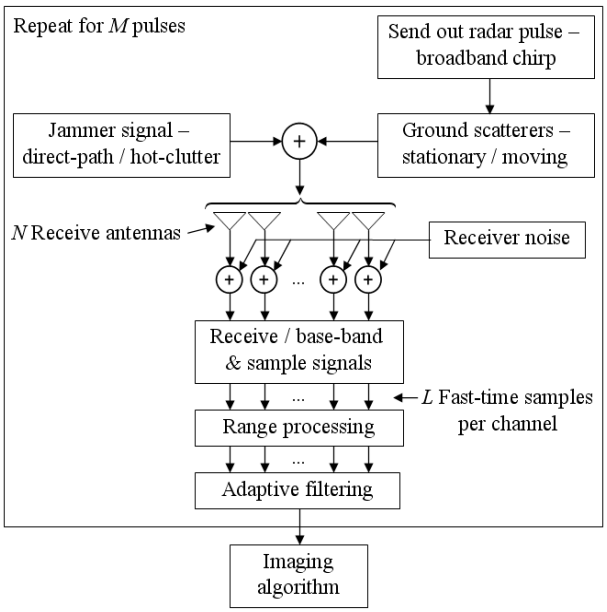

Figure 1: SAR processing diagram

2.2 Jammer model

The bistatic jammer model assumes there are K HC patches within a given area. If an absolute time variable, $\tilde{t} = u/v_p + t$ is defined as the sum of slow-time and fast-time, the interference plus noise signal is formed by the superposition of the direct path, hot-clutter scatterers and the receiver noise,

$$q_n(t,u) = \sum_{k=0}^{K} b_k J(\tilde{t} - \bar{\tau}_{n,k}(t,u)) \exp[-j\omega_c \bar{\tau}_{n,k}(t,u)] \exp[-j\omega_{d,k} t] + \nu_n(t,u) \tag{3}$$

where $J(\cdot)$ is the jamming signal waveform, $\bar{\tau}_{n,k}(\cdot)$ is the bistatic delay for the k^{th} scatterer, $\omega_{d,k}$ is the fast-time doppler frequency and b_k is defined as the relative magnitude between the direct-path and hot-clutter signal. The zero index refers to the direct-path with $b_0 = 1$.

The power spectral density of the jammer signal has an apparent bandwidth B, centred at baseband with power level, σ_J^2. Realisations of the jammer signal $J(\cdot)$ can then be generated by an eigen-decomposition of the jammer autocovariance,

$$r_J(\tau) = \sigma_J^2 \operatorname{sinc}(B\tau) \tag{4}$$

A physically based model for the multipath scattering is presented by Beckman, [6] and uses a surface roughness parameter K_β to define the scattering distribution between the SAR and an airborne jammer at heights h_P and h_J respectively, separated by a distance $\tilde{x}_J$ in the ground plane. The coefficients, $b_k = \rho B_k$ for $k > 1$ are formed with a HC scaling factor ρ, relative to the direct-path and a random amplitude B_k, determined from the scattering model.

3 Fast-time Filtering

For effective fast-time filtering, the fast-time sample rate, Δ_t is oversampled by a factor of two to provide increased correlation, [7]. Spatial beamforming for the l^{th} fast-time range bin requires stacking of both the received data and the signal model to form $N \times 1$ spatial vectors,

$$\mathbf{x}(t_l,u) = [x_{-(N-1)/2}(t_l,u), \ldots, x_{(N-1)/2}(t_l,u)]^T,$$
$$\mathbf{s}(u) = [s_{-(N-1)/2}(u), \ldots, s_{(N-1)/2}(u)]^T$$

where $t_l = l\Delta t$. Beamforming is then performed by matching the received data vector with the spatial steering vector,

$$y(t_l,u) = \mathbf{s}^H(u)\mathbf{x}(t_l,u) \tag{5}$$

To extend the processing to use fast-time taps, the spatial data vector is stacked over the future $\tilde{L} < L$ taps,

$$\mathbf{X}(t_l,u) = \left[\mathbf{x}^T(t_l,u), \mathbf{x}^T(t_{l-1},u), \ldots, \mathbf{x}^T\left(t_{l-\tilde{L}+1},u\right)\right]^T$$

with data components for $l < \tilde{L}$ set to zero. The fast-time component of the steering vector post range processing is given by,

$$g_k = \operatorname{sinc}\left[B(k-1)\Delta_t\right], \qquad k = 1 \ldots \tilde{L} \tag{6}$$

and can be stacked to give the fast-time steering vector,

$$\mathbf{g} = [g_1, \ldots, g_{\tilde{L}}]^T \in \mathcal{C}^{\tilde{L}\times 1} \tag{7}$$

If no oversampling is used, the fast-time model matches the delta function commonly used in literature, [2] where it is assumed that the target occupies a single range bin. The fast-time filter is then represented as a convolution,

$$\tilde{y}(t_l,u) = \mathbf{S}^H(u)\mathbf{X}(t_l,u) \tag{8}$$

with the space/fast-time steering vector formed by the Kronecker product of the spatial and temporal steering vectors,

$$\mathbf{S}(u) = \mathbf{g} \otimes \mathbf{s}(u) \in \mathcal{C}^{\tilde{L}N\times 1} \tag{9}$$

3.1 Generalised Sidelobe Canceller

The reduced rank GSC is a beamspace STAP implementation and is shown in Figure 3.1. It forms a set of 'beams' with the main beam in the 'desired' target direction and the other 'reference' beams going through a blocking matrix $\mathbf{B}(u)$ to remove the desired signal from the data. The reference beams are then transformed with the matrix $\mathbf{U}(u)$ to reduce rank, filtered and subtracted from the main beam. For this application, the GSC is preferred over the traditional element space processor as it is better suited for applying reduced rank transforms, [8].

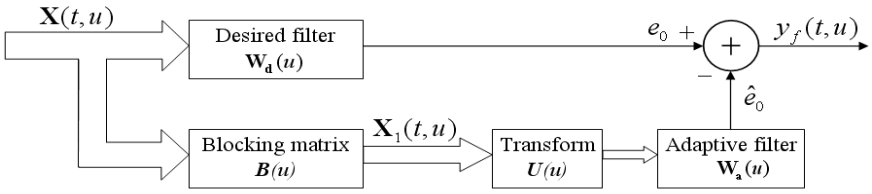

Figure 2: Reduced rank GSC

The output of the GSC is given by,

$$\begin{aligned} y_f(t,u) &= \mathbf{W}_{\text{d}}^H(u)\mathbf{X}(t,u) - \mathbf{W}_{\text{a}}^H(u)\mathbf{U}^H(u)\mathbf{B}^H(u)\mathbf{X}(t,u) \\ &= \left[\mathbf{W}_{\text{d}}(u) - \mathbf{B}(u)\mathbf{U}(u)\mathbf{W}_{\text{a}}(u)\right]^H \mathbf{X}(t,u) \end{aligned} \tag{10}$$

where the desired weight is given by

$$\mathbf{W}_{\text{d}}(u) = \mathbf{C}(u)\left[\mathbf{C}^H(u)\mathbf{C}(u)\right]^{-1}\mathbf{D} \in \mathcal{C}^{\tilde{L}N\times 1} \tag{11}$$

with $\mathbf{C}(u)$ containing the N_{con} adaptive constraints, usually expressed as a function of the steering vector with desired response, $\mathbf{D}$. To successfully remove the desired signal in the reference beam, the blocking matrix must to be orthogonal to the constraint matrix, $\mathbf{B}^H(u)\mathbf{C}(u) = 0$. A general method for the blocking matrix design has been presented in [3]. The adaptive weight vector of size $\tilde{L}(N - N_{\text{con}}) \times 1$ is designed to minimise the mean square error between $\hat{e}_0$ and e_0, with the solution given by [5],

$$\begin{aligned} \mathbf{W}_{\text{a}}(u) &= \left[\mathbf{U}^H(u)\mathbf{B}^H(u)\mathbf{R}(u)\mathbf{B}(u)\mathbf{U}(u) + \eta\mathbf{I}\right]^{-1} \\ &\quad \mathbf{U}^H(u)\mathbf{B}^H(u)\mathbf{R}(u)\mathbf{W}_{\text{d}}(u) \\ &= \left[\mathbf{U}^H(u)\mathbf{R}_{X_1}(u)\mathbf{U}(u) + \eta\mathbf{I}\right]^{-1}\mathbf{U}^H(u)\mathbf{r}_{X_1,e_0}(u) \end{aligned}$$

where $\mathbf{R}_{X_1}(u)$ and $\mathbf{r}_{X_1,e_0}(u)$ are the reference covariance and cross-covariance respectively and the diagonal loading level, η acts to improve the robustness by smoothing the adaption via compression of the eigenvalues, [9]. The normalised interference plus noise covariance matrix $\mathbf{R}(u) = \alpha\mathbf{R}'(u)$ is determined by averaging over L_{t} range bins,

$$\mathbf{R}'(u) = \frac{1}{L_{\text{t}}}\sum_{l=1}^{L_{\text{t}}}\mathbf{Z}(t_l,u)\mathbf{Z}^H(t_l,u) \in \mathcal{C}^{\tilde{L}N\times\tilde{L}N} \tag{12}$$

with the normalising value, $\alpha = \text{Tr}\left\{\mathbf{R}'(u)\right\}/(\tilde{L}N)$ provides a relative measure of the effect of diagonal loading. It is assumed techniques described in [10] can be used to get different realisations of the interference plus noise signal without any targets present. The interference plus noise vector, $\mathbf{Z}(\cdot)$ is formed similarly to the data vector $\mathbf{X}(\cdot)$.
The spatial constraint matrix used for this study has a unity response in the steering direction with its first derivative equal to zero. This has shown to be effective as it allows less potential signal suppression [3].

$$\mathbf{c}(u) = \left[\mathbf{s}(u), \frac{\partial\mathbf{s}(u)}{\partial\theta(u)}\right]^T \quad ; \quad \mathbf{d} = [1,0]^T \tag{13}$$

Note, that if only the steering vector constraint is used, the adaptive processor is known as the Minimum Variance Distortionless Response (MVDR). The spatial constraints are related to the space/fast-time versions by,

$$\begin{aligned} \mathbf{C}(u) &= \mathbf{I}_{\tilde{L}} \otimes \mathbf{c}(u) \in \mathcal{C}^{\tilde{L}N\times\tilde{L}N_{\text{con}}} \\ \mathbf{D} &= \mathbf{g} \otimes \mathbf{d} \in \mathcal{C}^{\tilde{L}N_{\text{con}}\times 1} \end{aligned} \tag{14}$$

3.2 Reduced Rank Transform

The choice of transform, $\mathbf{U}(u)$ can be found by an eigen-decomposition of the reference interference plus noise covariance matrix,

$$\mathbf{R}_{X_1}(u) = \mathbf{Q}\boldsymbol{\Lambda}\mathbf{Q}^H \in \mathcal{C}^{\tilde{L}(N-N_{\text{con}})\times\tilde{L}(N-N_{\text{con}})}, \tag{15}$$

and choosing C eigenvalue/eigenvector pairs, $(\lambda_c, \mathbf{q}_c)$ according to a ranking criteria. If the eigen-pairs are ranked according the eigenvalues, the transform is given by,

$$\mathbf{U}_{\text{PC}}(u) = [\mathbf{q}_1, \ldots, \mathbf{q}_C] \in \mathcal{C}^{\tilde{L}(N-N_{\text{con}})\times C} \tag{16}$$

This is known as Principle Component (PC) decomposition and the GSC will retain full adaptive performance if C is greater than the rank of $\mathbf{R}_{X_1}(u)$. A second criteria is known as the cross-spectral metric (CSM) and utilises knowledge of the constraint vector to suppress the strongest interference in the mainbeam, [8]. This is achieved by decomposing $\mathbf{R}_{X_1}(u)$ according to Equation 15 and selecting the C largest eigen-pairs according to the CSM, i.e.,

$$\rho_c = \frac{|\mathbf{q}_c\mathbf{r}_{X_1,e_0}(u)|^2}{\lambda_c} \tag{17}$$

With this ranking, the CSM transformation is given by,

$$\mathbf{U}_{\text{CSM}}(u) = [\mathbf{q}_{\rho_1}, \ldots, \mathbf{q}_{\rho_C}] \in \mathcal{C}^{\tilde{L}(N-N_{\text{con}})\times C} \tag{18}$$

where $(\lambda_{\rho_c}, \mathbf{q}_{\rho_c})$ denotes the c^{th} eigen-pair with λ_{ρ_1} the largest eigenvalue, λ_{ρ_2} the second largest, and so on. Using either of these approaches, the reduction in computational complexity of the matrix inverse is reduced from $\text{O}(\tilde{L}(N - N_{\text{con}}))^3$ to $\text{O}(C)^3$.

4 Simulated Results

A multichannel X-band SAR simulation has been implemented in MATLAB with parameters summarised in Table 1. A sample image is used for comparison with image formation performed with a spatial matched filter interpolation algorithm.

Table 1: Simulation parameters

Parameters	**Value**
Carrier frequency (f_c) / bandwidth (B)	10 / 0.3 GHz
Number of elements (N) / spacing (δ)	5 / $\frac{\lambda}{2}$ m
Number of pulses (M) / range bins (L)	100 / 250
Range centre (X_c) / clutter noise ratio	10 km / 20 dB
Range / azimuth resolution	1 / 5 m
Fast-time sampling (Δ_t) / training size (L_{t})	$\frac{1}{2B}$ / $3\tilde{L}N$
SAR height (h_P) / jammer height (h_J)	3 / 3 km
Jam. offset $(\tilde{x}_J)$ / jam. power (σ_J^2)	50 km / 80 dB
No. HC scats. (K) / relative HC scaling (ρ)	200 / 0.6

A moderately diffuse scattering scenario is used with $K_\beta = 0.4$ and to demonstrate the worst case scenario, both the direct and HC paths are incident in the SAR mainbeam spread over the range of angles, -0.7^o to 0.7^o. Based on the size of $\mathbf{R}_{X_1}(u)$ when $\tilde{L} = 15$ taps are used, the full interference rank for the MVDR constraint is 60 and for the derivative constraint is 45. The reference beam eigen-distribution is shown in Figure 3 with the normalised noise floor at $1/\alpha$ = -115dB. The eigen-distributions for both cases are nearly full rank and it is expected that the compression gained by diagonal loading will achieve better reduction in rank.

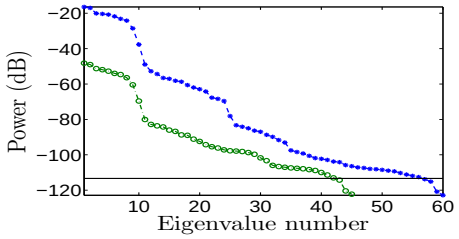

Figure 3: Reference beam eigen-distribution for: (- -) MVDR constraint, (-.-) derivative constraint

The adaptive performance is measured by the Signal Distortion Ratio (SDR) which is a measure of the signal power of the adapted image relative to an ideal image with no interference present. With no adaption, the conventional SDR is 3.8dB. However the first results in Figure 4 show the full rank GSC with $C = \tilde{L}N$ and the SDR improvement gained by using fast-time taps. The plot of the left is with the MVDR constraint and the one on the right uses derivative constraints. With -60dB of diagonal loading and 15 fast-time taps, the MVDR SDR improves from 4 to 6.5dB. The derivative constraint SDR however reaches a maximum 7.1dB and maintains this level between -90dB to -60dB of diagonal loading. The next two Figures 5-6 show how the SDR varies as a function of the GSC rank and the level of diagonal loading. The plots on the left are the PC results and the plots on the right are the CSM. The MVDR results are very sensitive to diagonal loading and the CSM ranking criteria shows improved performance over PC only when the filter rank is low. Beyond this, there is little difference between the two ranking criteria as the filter rank approaches the full rank results in Figure 4. Results for the derivative constraints however are not as greatly affected by the diagonal loading level. With a filter rank of only 10 and a small amount of diagonal loading, this filter can safely achieve the same SDR level as the full rank case.

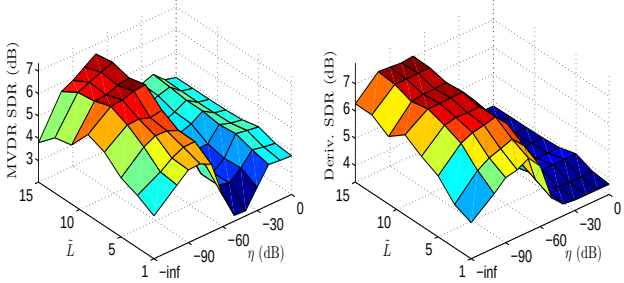

Figure 4: SDR for full rank GSC with varying $\tilde{L}, \eta$

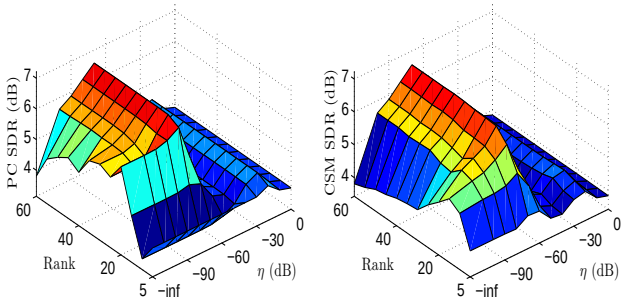

Figure 5: SDR for MVDR constraint with varying rank, η

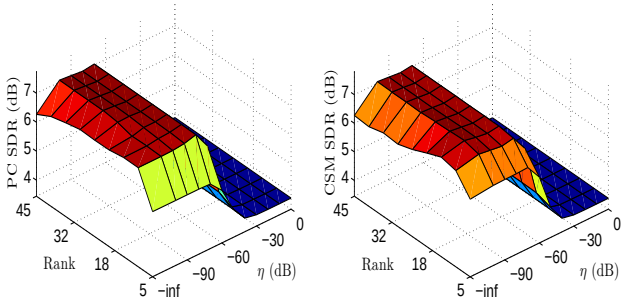

Figure 6: SDR for deriv. constraints with varying rank, η

5 Conclusion

This paper has shown how the constrained fast-time GSC can be formulated with reduced rank and computational complexity using transforms based on the PC and CSM decompositions. These use the adaptive degrees of freedom more effectively to remove the hot-clutter interference and not distort the final SAR image.

References

[1] L. Rosenberg and D. Gray. Anti-jamming techniques for multichannel SAR imaging. In *To appear in IEE Proceedings of Radar, Sonar and Navigation*, April 2006.

[2] D. Rabideau. Clutter and jammer multipath cancellation in airborne adaptive radar. *IEEE Transactions on Aerospace and Electronic Systems*, 36(2):2909–2912, 2000.

[3] L. Rosenberg and D. Gray. Fast-time filtering with multichannel SAR. In *Adaptive Sensor Array Processing Workshop*, June 2005.

[4] H. N. Nguyen. *Robust Steering Vector Mismatch Techniques for Reduced Rank Adative Array Signal Processing*. PhD thesis, Virginia Polytechnic Institute and State University, 2002.

[5] A. M. Haimovich, C. Peckham, T. Ayoub, J. S. Goldstein, and I. S. Reed. Performance analysis of reduced-rank STAP. In *IEEE National Radar Conference*, pages 42–47, 1997.

[6] P Beckman. *The Scattering of Electromagnetic Waves from Rough Surfaces*. Pergamon Press Ltd., 1963.

[7] R. L. Fante and J. A. Torres. Cancellation of diffuse jammer multipath by an airborne adaptive radar. *IEEE Transactions on Aerospace and Electronic Systems*, 31(2):805–820, 1995.

[8] J. R. Guerci. *Space-Time Adaptive Processing for Radar*. Artech House, 2003.

[9] J. Ward, H. Cox, and S. M. Kogon. A comparison of robust adaptive beamforming algorithms. In *Asilomar Conference on Signals, Systems and Computers*, volume 2, pages 1340–1344, 2003.

[10] J. Ward. Space-Time Adaptive Processing for airborne radar. Technical report 1015, Lincoln Labs. MIT, 1994.